Comparison of engine models of UHBPR turbofan at high incidence

Andrea Magrini*
Università Degli Studi di Padova, via Venezia 1, 35131 Padova - Italy

Gokul Subbian†
Technische Universität Braunschweig, Hermann-Blenk-Str. 37, 38108 Braunschweig - Germany

Denis Buosi‡
Hit09 S.r.l., Piazzetta Bettiol 15, 35137 Padova - Italy

Sebastian Spinner §
German Aerospace Center, Lilienthalplatz 7, 38108 Braunschweig, Germany

Ernesto Benini¶
Università Degli Studi di Padova, via Venezia 1, 35131 Padova - Italy

Rolf Radespiel‖
Technische Universität Braunschweig, Hermann-Blenk-Str. 37, 38108 Braunschweig - Germany

Powered-on flight is typically simulated via 1D boundary conditions (BC) at the engine entry and exit planes of the computational domain. In this paper, we apply this standard approach and two flow-coupled blade models based on an actuator disk (AD) and a body force (BFM) model to an ultra-high bypass ratio turbofan at take-off condition. The results obtained with the BC are compared to the two rotating engine representations at increasing angle of attack. The AD calibrated from 3D CFD solutions exhibits a deficit of mass flow and fan stage total pressure ratio impacting the prediction. In the investigated regime, the flow field obtained is generally homogeneous between BC and BFM, since no inlet stall has developed. The exhaust flow shows the largest differences, due to the non-uniform work input and mass flux generated by the coupled blade models, mainly due to the pylon backpressure. Engine characteristics are qualitatively captured in the AD, although influenced by the integral metrics deviation. Code-to-code comparison between Ansys Fluent and DLR TAU solver with the BC model indicates close agreement.

I. Introduction

Computational simulations of full aircraft configurations represent nowadays a viable and widespread method to obtain valuable information about the aircraft aerodynamics and estimate the propulsive performance of the powered vehicle. The progress in viscous Reynolds-Averaged Navier-Stokes (RANS) solvers, mesh generation, and experimental techniques has allowed researchers to gain increasing confidence in the numerical results and disclose several effects related to the interaction between the turbofan and the airframe [1–5]. In this specific field, numerous efforts have been put in the last years to analyse and improve the installation effects that characterise in particular the large size Ultra-High Bypass Ratio (UHBPR) engines envisaged to be adopted on a medium-term basis to reduce the environmental impact of the civil aviation sector [6].

In many numerical solutions of propulsion integration aerodynamics, the aircraft turbomachinery is excluded from the computational domain and represented by setting 1D Boundary Conditions (BC) on the fan face and nozzles entry

*Post-doc researcher, Department of Industrial Engineering
†Research-assistant, Institute of Fluid Mechanics,
‡Research Engineer
§Research Scientist, Institute of Aerodynamics and Flow Technologies
¶Full Professor, Department of Industrial Engineering
‖Director, Institute of Fluid Mechanics

planes. This way, the mass flow rate, the Fan Nozzle Pressure Ratio (FNPR) and the Core Nozzle Pressure Ratio (CNPR) can be easily controlled to match the thermodynamic design specification coming from cycle analysis. In this approach, the engine operating point is decoupled from the external aerodynamics. The mass flow rate at the fan inlet is fixed. The mass flow through the bypass and core nozzles can only vary if they are not choked, but no conservation from the fan inlet to the nozzle outlet is automatically achieved if not explicitly enforced. In addition, the boundary distributions are evenly set. This representation, although very practical from a numerical point of view, gives only a one-dimensional static and decoupled representation of the turbomachinery, which can be a good approximation near the design condition and with uniform inflow and outflow conditions.

If one of these factors are not met, i.e., off-design operation is considered or either the fan inlet flow or the nozzle backpressure are distorted, the engine will shift its operating point in order to restore, from an integral point of view, the balance of mass, momentum and energy. Clearly, this can only be captured in the numerical environment with a more complex model that actually reproduces the basic behaviour of a blade row. Different options have been devised to include the effect of the compression row in the numerical domain without having to simulate directly the whole three-dimensional cascade. Among these, one of earliest approaches was the Actuator Disk (AD) method, which is based on the blade element theory of Glauert and was originally conceived for propellers. The concept has been extended to more complex cases, like axial transonic fans, as a way of improving the flow field prediction where the fan/airframe interaction is relevant [7–10].

Tackling an alternative representation with a low computational cost, throughflow methods have also been developed. Among them, the Body Force Model (BFM) approach replaces the solid blades with a force distribution amounting to the same momentum and energy exchange of the blades onto the fluid, in a circumferential average meaning [11]. BFM can be thought of as a non-axisymmetric throughflow, where viscous losses and blockage effects can be accounted for, reaching close match of time-averaged unsteady RANS (URANS) simulations of full-wheel configurations [12–14].

In this paper, we aim to compare the three aforementioned methods for the simulation of an ultra-high bypass ratio turbofan with a flight model nacelle and pylon in isolation. During take-off and high incidence operation, the rotation of the streamtube from the freestream to the engine axis introduces a nonuniform inflow condition that cannot be completely eliminated by the intake. Similarly, the backpressure on the nozzle exit sections can be uneven because of incidence effects or exposed high-lift devices, changing the turbofan operating point when the nozzle is unchoked. For this reason, assessing the impact of the modelling approach in this flight phase appears useful to determine whether the standard practice is sufficient to estimate the aerodynamic performance, or whether it deviates from the more faithful engine representations. This is particularly important for UHBPR turbofans, whose airframe integration needs to be tightened because of their large diameters making the underwing accommodation more challenging over several aspects. By analysing the isolated nacelle with pylon configuration, the differences between the models can be attributed solely to the engine representation method, making their comparison fair and more clearly comprehensible. The paper thus addresses the computational simulation of the isolated nacelle and pylon using one-dimensional Boundary Conditions (BC), Actuator Disk (AD), and Body Force Model (BFM) to represent powered-on conditions and evaluate the differences between the three models. Moreover, it provides a code-to-code comparison between the DLR TAU solver and the commercial solver ANSYS Fluent in the case of BC.

The paper is organised as follows: the Case Study section presents the geometry employed in the analysis. Numerical methods and details of the engine representation models are given in section Methods. Finally, the results of the computational simulations are discussed in section Results.

II. Case Study

The test case considered for the analysis is an UHBPR turbofan engine representative of a state-of-the-art geared architecture for low specific thrust and fan pressure ratio. The turbomachinery is installed in a flight model nacelle designed to be mounted under the NASA Common Research Model (CRM) [15] wings at the Aerodynamic Design Point (ADP) condition of Mach number M = 0.85 cruise at an altitude of 10668 m. The geometry was drawn from indications reported in the open literature and a preliminary design space exploration and features a short and compact cowl to reduce the overall drag. It was used as a baseline configuration for successive improvements of the installed performance in a complex multilevel optimisation procedure within the IVANHOE project [16–18]. Starting from thermodynamic specifications of the engine cycle at the ADP, an UHBPR fan with OGV bypass stage was designed. The blade geometries were necessary for the application of the two modelling approaches, as described in the next section. The operating conditions of the study are summarised in Tab. 1 and pertained to the take-off phase with low speed and increasing angle of attack.

Table 1 Operating Conditions.

Quantity	Value
Altitude [m]	0
Mach Number	0.26
Temperature [K]	ISA+15
Angle of Attack [deg]	0, 6, 12, 16

III. Methods

A. Computational Model

The computational model for the simulations had been developed throughout the IVANHOE project by combining data from axisymmetric nacelle validation test cases and indications coming from the Drag Prediction Workshops (DPW) series promoted by the AIAA [19], where different meshing strategies for the NASA CRM were compared to provide gridding guidelines [5]. The model comprised the UHBPR nacelle geometry with the pylon, inserted into a rectangular block whose farfield boundary was located 100 highlight radii far away. The hybrid mesh, made up of an anisotropic structured boundary layer with $y^+ < 1$ and tetrahedral cells in the external flow region, featured nested refinement blocks surrounding the nacelle to capture the streamtube diffusion and the jet expansion. A cut view of a coarse grid illustrating the topology is depicted in Fig. 1. Validation of the computational approach and grid sensitivity analyses for the isolated and installed configurations can be found in previously given ref. [16, 17].

The nacelle geometry was delimited by the engine characteristic planes, where boundary conditions were specified in the BC approach: the fan face plane, set as a pressure outlet with a target mass flow; the bypass nozzle inlet, set as an inflow boundary with total pressure and temperature specification; the core nozzle inlet, set as the same type of bypass nozzle inlet. The internal engine region, not present in the BC simulations, was filled with the bypass stage mesh in the AD and the BFM models described in the next sections. The structured block was connected to the external domain via a numerical interface. This way, the same mesh for the nacelle was retained equal for the three approaches, thus eliminating any potential influence on the results. The computational fluid dynamics simulations were carried out using two flow solvers. The AD model was implemented into the DLR TAU solver [20], while the BFM was implemented into the commercial solver Ansys Fluent [21]. The $\kappa - \omega$ *SST* turbulence closure was selected, based on the validation of the NASA CRM data. As anticipated, the BC simulations were run with both solvers, providing a reference to compare the coupled engine models with.

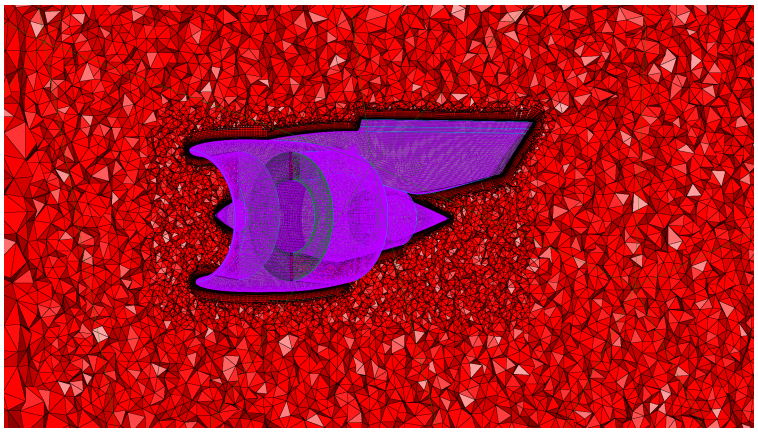

Fig. 1 Example of a coarse grid around the nacelle and pylon.

B. Actuator Disk model

Actuator-disk (AD) methods were initially conceived to model propeller flows [22]. The procedure replaces the blade row with an infinitely thin disk, through which a discontinuous pressure jump is realised, but the velocity remains

continuous. According to the blade element approach, the lift and drag forces exerted by the blades on the fluids are estimated using look-up tables of lift and drag polars obtained for different isolated blade sections at varying incidence. The forces are thus redistributed along the disk surface using the local incoming flow direction. In the present application, a finite volume version of the model that adopts a conservative flux formulation [23] implemented into the DLR software TAU was used. The calibration data are extracted from RANS solutions of the blade row [10] and are interpolated on each cell of the CFD grid to supply the forces that drive the flow through the disk. Therefore, the model relies on blade-to-blade CFD solutions of rotor and stator and necessitates a detailed knowledge of the geometry. The local blade angle of attack is computed neglecting radial components and used to derive the lift and drag coefficients taken from a lookup table. Data are given at a limited number of span sections from hub to shroud and then radially interpolated in the intermediate positions. Force blanking was adopted near the endwalls. The full velocity vector is employed to find the dynamic pressure to compute the forces from the non-dimensional coefficients.

In the current implementation, according to the blade element theory, lift and drag coefficients were taken directly from quasi 2D streamwise flow sections along the span of 3D blade computations of fan and OGV blades. Variation of the incoming incidence was obtained by considering the full speedline of the stage, from choking to stall. In this way, radial effects occurring along the blade span could be incorporated in the extracted polar. A possible drawback of such approach is that the incidence range of the polar might not completely cover those found locally when the stage is installed in the nacelle, as it will be highlighted in the Results section.

C. Body Force Model

As mentioned in the introduction, the body force method relies on the replacement of a solid metal blade row with a distribution of forces that represents the circumferential-averaged effect of the cascade on the fluid. This way, the volume swept by the blades is simulated by adding momentum and energy source terms to the right-hand side of the RANS equations, that generate the compression and the suction of the turbomachinery. The forces can be decomposed into a flow-normal and a flow-parallel component, the first one responsible for the flow turning, the second for the increase of entropy and the loss generation. Different BFM formulations have been developed in the last years, providing semi-analytic models of these two components [24–27]. The inclusion of a blockage factor accounting for the blade thickness improves the prediction of transonic flows, by adding additional source terms to the equations [28].

The model employed in the study derives from the Lift/Drag method of Thollet [26]and has been used in other researches related to UHBPR nacelles [29, 30]. Details of the current implementation and experimental validation are given in [31]. The BFM represents a local formulation of the AD, where lift and drag are given along the blade mean camberline, rather than lumped on the blade element chord. As in Fig. 2, the flow normal (f_n) and parallel (f_p) force components, relative to the velocity $\vec{W}$, are expressed as a function of local flow variables, local blade geometry, and local calibration coefficients that are extracted from a standard 3D single passage steady simulation of the solid blade row. The force field is computed for each cell inside the blade region and the corresponding source terms in the RANS equations are calculated and added during the flow solution, including the metal blockage effect. Like in the AD approach, this BFM version requires the knowledge of the cascade geometry since it is instructed from higher fidelity simulations.

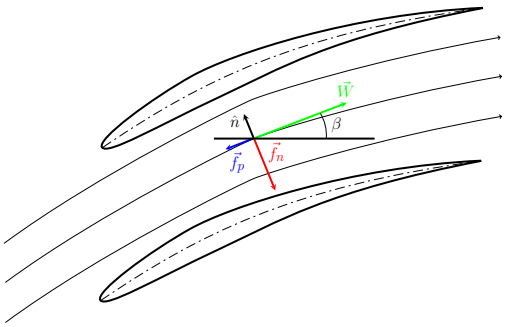

Fig. 2 Body force model concept. Forces exerted by the blade are decomposed along the flow normal and flow parallel direction and injected into the volume swept by the blade without modelling the solid row. Adapted from [31].

IV. Results

The results of the take-off simulations at increasing angle of attack with the three engine models and two flow solvers are here presented in terms of flow field and fan stage status. It must be kept in mind that unlike the BC approach, with the AD and BFM the engine mass flow for a given rotational speed depends on the coupling between the blade models and the external solution. For this reason, and also given the fact that the boundary distributions are not uniform, the mass flow can deviate from the 1D prescription and be different from the one initially obtained in the decoupled simulation. The magnitude of this deviation is by itself an indication of the approximation of the BC model and the input data used.

A. Flow field

Among the different angles of attack, solution data are here examined at the highest incidence only. In fact, the same features that will be discussed at 16° were present also at lower angles, due to the attached field spectrum. A main observation is a reduction of mass flow and fan pressure ratio with the AD model, that impacted all obtained flow fields. Such feature was inherent to the AD, being present at all angles of attack, and will be further explained in Sec. IV.B.

With this premise, the Mach number contours on a vertical plane cutting the engine axis at $\alpha = 16°$ is illustrated in Fig. 3 for the two BC simulations, the AD, and the BFM model. On the intake side, due to the high angle of incidence, a strong acceleration past the lower lip can be observed. In Fig. 3c, a lower overspeed region is present in the AD due to the reduced mass flow. On the exhaust, TAU and Fluent BC present similar jet characteristics. The Mach number in the fan stream of the BFM appears lower in the shown section, which comes from a more non-axisymmetric expansion due to the nonuniform nozzle entry status caused by the pylon, as it will be discussed later. In the AD, the fan stage operates with a lower mass flow and pressure ratio, resulting in a lower acceleration of the jet. Another observation is the influence of the pylon in the upper half core exit channel, through which the flow experiences higher acceleration in comparison to the lower half channel.

The uneven distribution of stagnation parameters achieved with coupled models can be better appreciated in Fig. 4, showing the equatorial plane for the same angle of attack. The inlet flow appears uniform in both inboard and outboard, due to geometrical symmetry of the nacelle and no sideslip angle. In the BC, Fig. 4a-4b, the discharge flow is also completely symmetrical because of the 1D boundary specification. For the AD model, Fig. 4c, the upper side exit flow in the figure has a mildly higher velocity than the lower side, whereas the BFM model of Fig. 4d has an opposite distribution. However, this planar cut view parallel to the engine axis can magnify some features in the jet, since its boundaries are not axisymmetric and slightly differ between the models.

Surface pressure distribution around the nacelle is shown in Fig. 5 for $\alpha = 6$, 12, and 16°. Lines with higher suction peaks correspond to the keel section and lines with slightly lower suction values to the crown section, on the vertical symmetry plane. Increase in suction peak with respective growth in angle of attack can be clearly seen. BFM and BC exhibit good overlapping, which is due to the equivalence of the inlet mass flow rate, as reported later. The AD has a qualitatively similar behaviour, though influenced by the lower flow rate, that reduces the suction peaks around the leading edges. Moreover, in the internal engine duct, it can be observed the diminished compression achieved compared to the BFM. The largest difference occurs on the bypass nozzle. The portion from the BC plane to the pylon leading edge falls in $x/l = [0.65, 0.7]$. There, the BFM curve does not match the BC, but the initial and final values are close. The AD has a higher static pressure, because of the reduced total pressure rise imparted. On the keel section, the bypass nozzle is clean and the outer wall pressure coefficient from $x/l = 0.65$ to $x/l = 1.0$ is closer between the three models. The BFM and AD curve shapes are similar, while in the BC a higher concavity is present. This comes from the fact that the boundary layer is fully developed in the blade models, whereas the flow has just entered the computational model in the BC. Moreover, the nozzle entry plane distribution is not even in the AD and BFM, owing to the pylon and the modest inlet swirl caused by the high incidence, resulting in a non-uniform work input from the rotor.

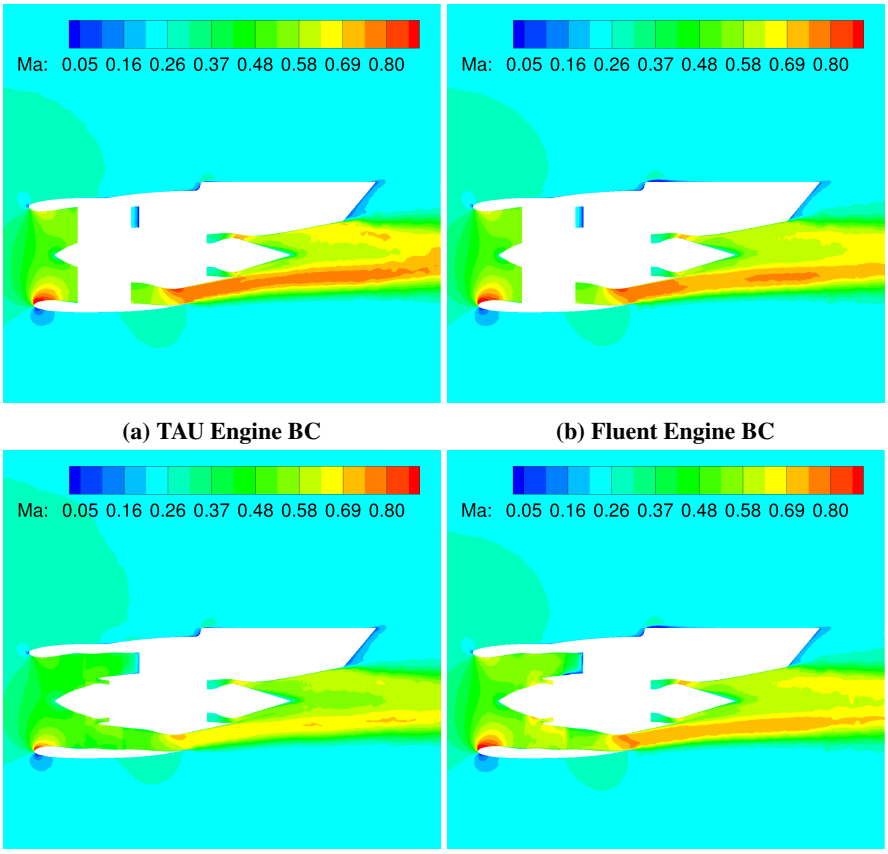

(a) TAU Engine BC **(b) Fluent Engine BC**

(c) TAU Actuator Disk **(d) Fluent Body Force Model**

Fig. 3 Flow characteristic through the nacelle. Vertical symmetry plane at α = 16°.

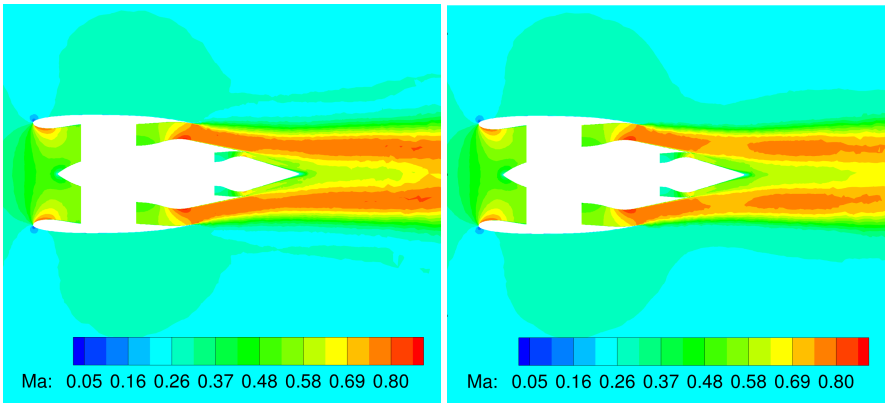

(a) TAU Engine BC **(b) Fluent Engine BC**

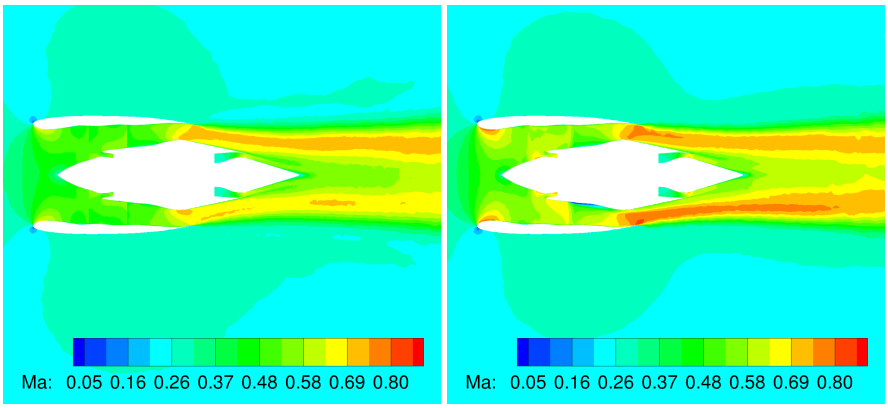

(c) TAU Actuator Disk **(d) Fluent Body Force Model**

Fig. 4 Flow characteristic through the nacelle. Horizontal symmetry plane at α = 16°.

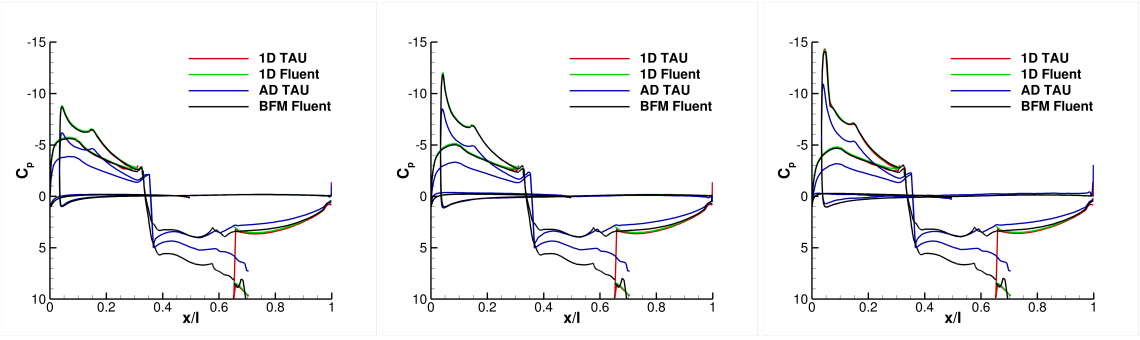

(a) α = 6° **(b) α = 12°** **(c) α = 16°**

Fig. 5 Surface pressure distribution in the nacelle at crown and keel sections.

B. Engine operating conditions

The engine operating conditions predicted by the AD and BFM models are here compared to analyse the difference in terms of integral performance metrics previously reported. As mentioned before, the AD mass flow rate and total pressure rate were computed to be lower than the expected fan stage performance. Figure 6 illustrates the normalised total pressure ratio before OGV in the BFM and AD and after the OGV for all models. In the first section, the top left part of the circle in Fig. 6b shows a larger total pressure, coming from the potential effect of the pylon propagating upstream and shifting the fan operating point towards higher work input and lower mass flux. The AD in Fig. 6a also presents a moderately higher compression on a region extending from top left to bottom right. However, the effect is less pronounced and the distribution is symmetric. In fact, the implementation of the AD model into TAU solver was done with the fan blades devised to rotate in the opposite direction, compared to the BFM, due to the model sign convention. Past the OGV, Fig. 6c-6d, the total pressure distribution remains substantially unaltered, especially in the AD. On the same section, boundary values were specified in the BC approach, thus appearing as uniform in Fig. 6e-6f.

From the shown figures, the lower compression of AD can be readily recognised. A summary of average integral metrics of the fan stage is given in the bar charts of Fig. 7. All data are normalised by the corresponding BC value at 0° of incidence. The Fluent solution of BC is reported, since no difference with TAU could be appreciated. The mass flow rate of the AD is 90% of those set in the BC and given from thermodynamic cycle analysis, Fig. 7a. Conversely, the UHBPR fan stage, built to meet the cruise aerodynamic design point, closely matches the cycle prediction at take-off, with a 1% lower stage Total pressure Ratio (TPR), Fig. 7b. The AD produces a 2.5% lower compression and a 7% lower Total Temperature Ratio (TTR). It appears to operate at an equivalent lower rotational speed, producing a proportional reduction of all characteristic parameters. A possible cause of this mismatch might reside on a discrepancy of the AD calibration methodology. In fact, some cells in the AD region near the endwalls were found to operate on the boundary of the extracted blade element polars, which can compromise the overall accuracy of its prediction. This is because a blade section in isolation has a larger operating range than the one achieved by the full span blade, which is limited by the stall onset typically occurring at high span for a low aspect ratio fan. When running under installation, the combination of ingested streamtube pre-rotation and non-uniform exit static pressure at the OGV outlet caused by the pylon can induce locally out-of-range values in some cells for the incidence mapped in the lookup table. Therefore, in a future implementation the calibration procedure will be revise to ensure that the full range of installed operating conditions is covered. A relevant feature to observe is that both AD and BFM have a slightly varying trend at increasing incidence, differently from the BC where all value are set fixed. In fact, the blade models react to the boundary conditions to restore the mass and energy flux balance through the fan stage. Lastly, the Gross Propulsive Thrust (GPT) generated by the propulsor is shown in Fig. 7d. The BC and BFM trend appear similar, but the latter has a 2% lower value. In the AD, the thrust is only 80% because of the reduced mass flow and TPR. The trend of mild reduction at increasing α is also present, though with a less negative slope, compared to the other data.

V. Conclusions

The UHBPR turbofan engine mounted on an isolated nacelle with pylon has been simulated at take-off conditions with two flow solvers and three fan stage models. The main source of deviation was found in the AD not producing the expected total pressure rise and mass flow rate. The reason for this was attributed to the adopted calibration procedure, relying on 3D blade simulations, rather than blade-to-blade analysis. The flow field over the nacelle external cowl and the intake is highly sensitive to the inlet mass flow rate. The equivalence of this parameter in the BC and BFM ensured that the wall pressure distribution was closely matched, whereas the AD suffered from the lower mass flow, smoothing the suction peaks past the leading edge.

The nozzle flow was more different between the BC and blade models, mainly because of the non constant distribution of stagnation parameters along the radial and azimuthal direction. While the first coordinate accounts for the inherent blade characteristic and the specified vortex distribution, the variation along the second coordinate results from the reaction of the row to the non-uniform stage exit pressure imposed by the pylon. This feature was evident in the BFM and qualitatively present also in the AD, though with lower amplitude. The engine gross thrust was around 2% lower in the BFM, relative to the BC. The offset can be attributed to the 1% lower total pressure ratio of the fan stage. However, the trend of slight reduction of gross thrust at increasing incidence was quite close between the two models, with qualitative replication also in the AD.

Overall, when matching the average values on the boundaries, a good agreement in terms of flow field was found between the BFM and BC, with no change from Fluent to TAU. Such result refers to an incidence range where the inlet flow remains attached. At higher angles of attack, that can arise due to wing upwash in the maximum lift point, or

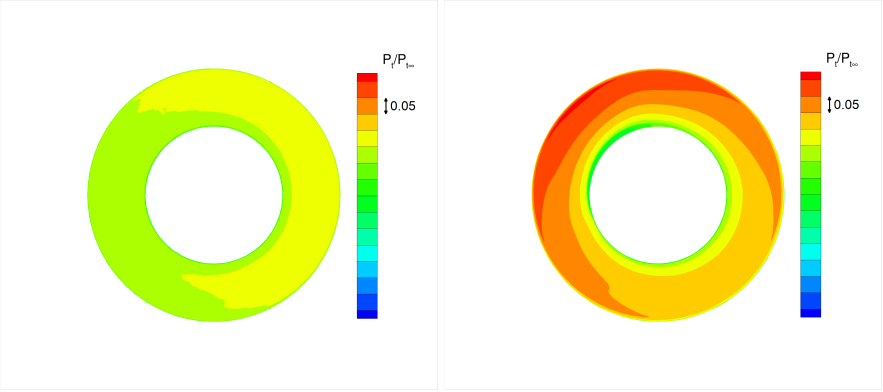

(a) TAU Actuator Disk - before OGV **(b) Fluent Body Force Model - before OGV**

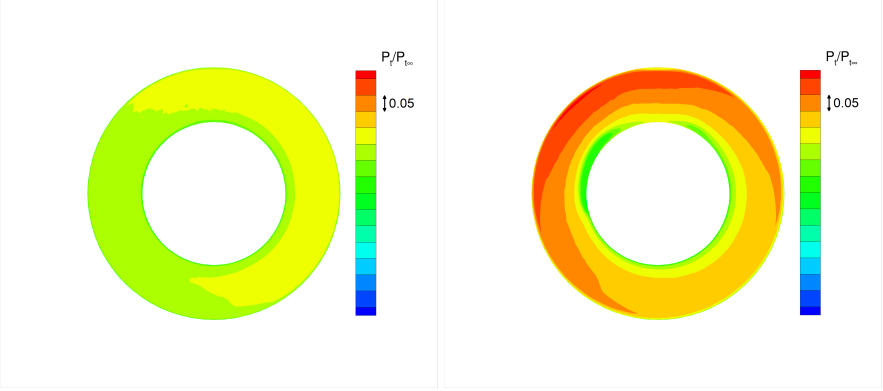

(c) TAU Actuator Disk - after OGV **(d) Fluent Body Force Model - after OGV**

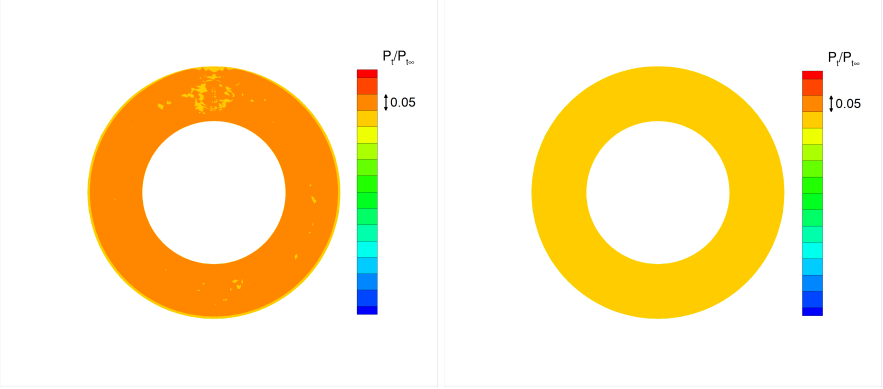

(e) TAU Engine BC - after OGV **(f) Fluent Engine BC - after OGV**

Fig. 6 Normalized total pressure ratio around OGV, α = 16°.

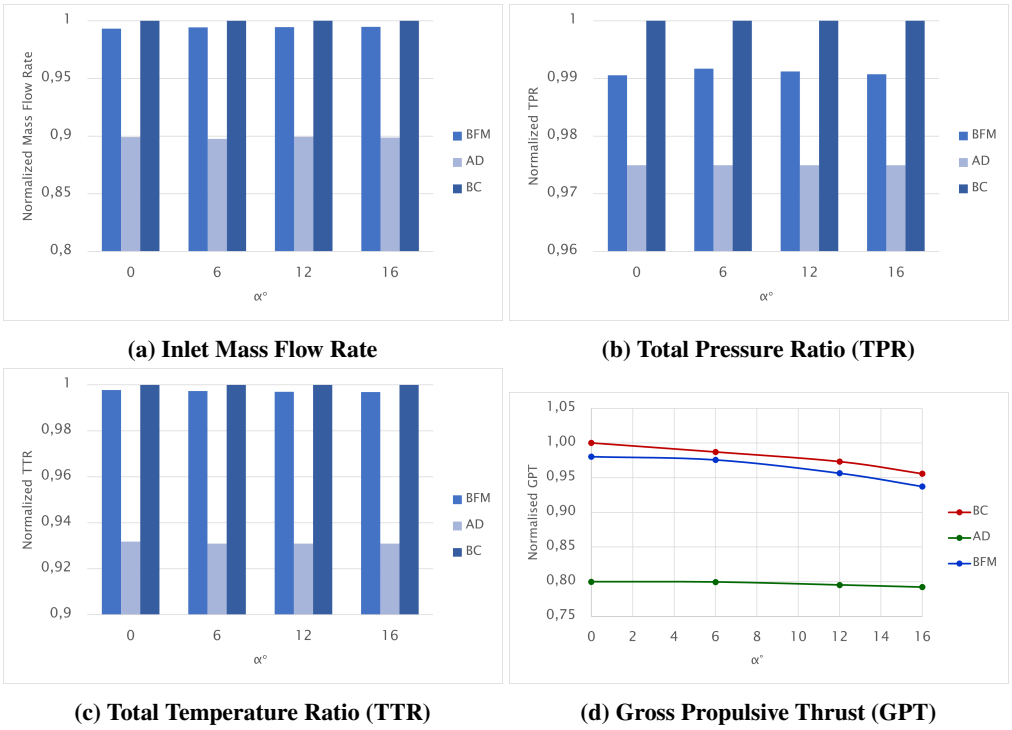

(a) Inlet Mass Flow Rate **(b) Total Pressure Ratio (TPR)**

(c) Total Temperature Ratio (TTR) **(d) Gross Propulsive Thrust (GPT)**

Fig. 7 Propulsor integral performance metrics variation at increasing angle of attack with the three models. Data are normalised by the corresponding BC value at $\alpha = 0°$.

in presence of crosswind, the deviations between the standard and decoupled models are expected to enlarge. Future continuation studies will address the improvement of the AD calibration to match the integral metrics prescribed by cycle analysis and the extension to more unfavourable regimes, also expanding the assessment in terms of propulsive forces.

Funding

This study is financed by the Clean Sky 2 project IVANHOE (Installed adVAnced Nacelle uHbr Optimisation and Evaluation). The project has received funding from the European Union's Horizon 2020 research and innovation programme under grant agreement number 863415.

TAU computations were performed using North German Supercomputing Alliance (HLRN)

References

[1] Rudnik, R., Rossow, C. C., and Geyr, H. F. V., "Numerical simulation of engine/airframe integration for high-bypass engines," *Aerospace Science and Technology*, Vol. 6, No. 1, 2002, pp. 31–42. https://doi.org/10.1016/S1270-9638(01)01139-7, URL https://www.sciencedirect.com/science/article/pii/S1270963801011397.

[2] Mani, M., Rider, B., Sclafani, A., Winkler, C., Vassberg, J., Dorgan, A., Cary, A., and Tinoco, E., "RANS Technology for Transonic Drag Prediction; A Boeing Perspective of the 4th Drag Prediction Workshop," *28th AIAA Applied Aerodynamics Conference*, 2010. https://doi.org/10.2514/6.2010-4221, URL https://arc.aiaa.org/doi/abs/10.2514/6.2010-4221.

[3] Levy, D. W., Laflin, K. R., Tinoco, E. N., Vassberg, J. C., Mani, M., Rider, B., Rumsey, C. L., Wahls, R. A., Morrison, J. H., Brodersen, O. P., Crippa, S., Mavriplis, D. J., and Murayama, M., "Summary of Data from the Fifth Computational Fluid Dynamics Drag Prediction Workshop," *Journal of Aircraft*, Vol. 51, No. 4, 2014, pp. 1194–1213. https://doi.org/10.2514/1.C032389, URL https://doi.org/10.2514/1.C032389.

[4] Brodersen, O., and Crippa, S., *RANS-based Aerodynamic Drag and Pitching Moment Predictions for the Common Research Model*, Springer International Publishing, Cham, 2014, pp. 485–493. https://doi.org/10.1007/978-3-319-03158-3_49, URL https://doi.org/10.1007/978-3-319-03158-3_49.

[5] Tinoco, E. N., Brodersen, O. P., Keye, S., Laflin, K. R., Feltrop, E., Vassberg, J. C., Mani, M., Rider, B., Wahls, R. A., Morrison, J. H., Hue, D., Roy, C. J., Mavriplis, D. J., and Murayama, M., "Summary Data from the Sixth AIAA CFD Drag Prediction Workshop: CRM Cases," *Journal of Aircraft*, Vol. 55, No. 4, 2018, pp. 1352–1379. https://doi.org/10.2514/1.C034409, URL https://doi.org/10.2514/1.C034409.

[6] Magrini, A., Benini, E., Yao, H.-D., Postma, J., and Sheaf, C., "A review of installation effects of ultra-high bypass ratio engines," *Progress in Aerospace Sciences*, Vol. 119, 2020, p. 100680. https://doi.org/https://doi.org/10.1016/j.paerosci.2020.100680, URL http://www.sciencedirect.com/science/article/pii/S0376042120300920.

[7] Joo, W. G., and Hynes, T. P., "The Simulation of Turbomachinery Blade Rows in Asymmetric Flow Using Actuator Disks," *Journal of Turbomachinery*, Vol. 119, No. 4, 1997, pp. 723–732. https://doi.org/10.1115/1.2841182, URL https://doi.org/10.1115/1.2841182.

[8] Kim, S., Yang, S., Lee, D., Baftalovski, S., and Makarov, V., "Three-dimensional flow calculation around/through isolated nacelle with an actuator disk modeling," *35th Joint Propulsion Conference and Exhibit*, 1999. https://doi.org/10.2514/6.1999-2668, URL https://arc.aiaa.org/doi/abs/10.2514/6.1999-2668.

[9] L. Wiart; O. Atinault; J.-C. Boniface; Barrier, R., "Aeropropulsive Performance of the NOVA Configurations," *30th Congress of the International Council of the Aeronautical Sciences*, ICAS, Daejeon, Korea, 2016. URL http://www.icas.org/ICAS{_}ARCHIVE/ICAS2016/data/papers/2016{_}0092{_}paper.pdf.

[10] Spinner, S., Keller, D., Schnell, R., and Trost, M., "A Blade Element Theory Based Actuator Disk Methodology for Modeling of Fan Engines in RANS Simulations," *AIAA AVIATION 2020 FORUM*, 2020. https://doi.org/10.2514/6.2020-2749, URL https://arc.aiaa.org/doi/abs/10.2514/6.2020-2749.

[11] Godard, B., De Jaeghere, E., Ben Nasr, N., Marty, J., Barrier, R., and Gourdain, N., "A Review of Inlet-Fan Coupling Methodologies," 2017. https://doi.org/10.1115/GT2017-63577, URL https://doi.org/10.1115/GT2017-63577.

[12] Burlot, A., Sartor, F., Vergez, M., Méheut, M., and Barrier, R., "Method comparison for fan performance in short intake nacelle," *2018 Applied Aerodynamics Conference*, American Institute of Aeronautics and Astronautics, Reston, Virginia, 2018. https://doi.org/10.2514/6.2018-4204, URL https://arc.aiaa.org/doi/10.2514/6.2018-4204.

[13] Benichou, E., Dufour, G., Bousquet, Y., Binder, N., Ortolan, A., and Carbonneau, X., "Body Force Modeling of the Aerodynamics of a Low-Speed Fan under Distorted Inflow," *International Journal of Turbomachinery, Propulsion and Power*, Vol. 4, No. 3, 2019, p. 29. https://doi.org/10.3390/ijtpp4030029, URL https://www.mdpi.com/2504-186X/4/3/29.

[14] Awes, A., Dufour, G., Daon, R., Marty, J., Barrier, R., and Carbonneau, X., "Unsteady Body Force Methodology for Fan Operability Assessment under Clean and Distorted Inflow Conditions," *AIAA Scitech 2021 Forum*, AIAA, Reston, VA, 2021. https://doi.org/10.2514/6.2021-0388.

[15] Vassberg, J., Dehaan, M., Rivers, M., and Wahls, R., "Development of a Common Research Model for Applied CFD Validation Studies," *26th AIAA Applied Aerodynamics Conference*, 2008. https://doi.org/10.2514/6.2008-6919, URL https://arc.aiaa.org/doi/abs/10.2514/6.2008-6919.

[16] Magrini, A., Buosi, D., Benini, E., and Sheaf, C., "Ultra-high bypass nacelle geometry design space exploration," *AIAA SciTech 2021 Forum*, AIAA, Reston, VA, 2021. https://doi.org/10.2514/6.2021-0990, URL https://arc.aiaa.org/doi/abs/10.2514/6.2021-0990.

[17] Magrini, A., Buosi, D., and Benini, E., "Maximisation of installed net resulting force through multi-level optimisation of an ultra-high bypass ratio engine nacelle," *Aerospace Science and Technology*, Vol. 119, 2021, p. 107169. https://doi.org/https://doi.org/10.1016/j.ast.2021.107169, URL https://www.sciencedirect.com/science/article/pii/S1270963821006799.

[18] Magrini, A., Buosi, D., and Benini, E., "Analysis of installation aerodynamics and comparison of optimised configuration of an ultra-high bypass ratio turbofan nacelle," *Aerospace Science and Technology*, Vol. 128, 2022, p. 107756. https://doi.org/https://doi.org/10.1016/j.ast.2022.107756, URL https://www.sciencedirect.com/science/article/pii/S1270963822004308.

[19] Vassberg, J., "A Unified Baseline Grid about the Common Research Model Wing/Body for the Fifth AIAA CFD Drag Prediction Workshop (Invited)," *29th AIAA Applied Aerodynamics Conference*, 2011. https://doi.org/10.2514/6.2011-3508, URL https://arc.aiaa.org/doi/abs/10.2514/6.2011-3508.

[20] Kroll, N., Langer, S., and Schwöppe, A., "The DLR Flow Solver TAU - Status and Recent Algorithmic Developments," *52nd Aerospace Sciences Meeting*, 2014. https://doi.org/10.2514/6.2014-0080, URL https://arc.aiaa.org/doi/abs/10.2514/6.2014-0080.

[21] ANSYS, *ANSYS Fluent 19.2 Theory Guide*, ANSYS, Inc., 2018.

[22] Glauert, H., *The Elements of Aerofoil and Airscrew Theory*, Cambridge University Press, Cambridge, 1983. https://doi.org/10.1017/CBO9780511574481, URL http://ebooks.cambridge.org/ref/id/CBO9780511574481.

[23] Raichle, A., "Flux Conservative Discretization of the Actuator Disk Model as a Discontinuity Surface," Phd thesis, 2017.

[24] Gong, Y., "A computational model for rotating stall and inlet distortions in multistage compressors," Phd thesis, Massachusetts Institute of Technology, 1999.

[25] Hall, D. K., "Analysis of civil aircraft propulsors with boundary layer ingestion," Phd thesis, Massachusetts Institute of Technology, 2015.

[26] Thollet, W., "Body force modeling of fan-airframe interactions," Ph.D. thesis, Université de Tolouse - ISAE, 2017.

[27] Huang, J., Lv, Y., Xia, A., Zhang, S., Tuo, W., Xue, H., Sun, Y., and He, X., "Improved Body Force Model for Estimating Off-Design Axial Compressor Performance," *Energies*, Vol. 15, No. 12, 2022. https://doi.org/10.3390/en15124389, URL https://www.mdpi.com/1996-1073/15/12/4389.

[28] Thollet, W., Dufour, G., Carbonneau, X., and Blanc, F., "Body-force modeling for aerodynamic analysis of air intake – fan interactions," *International Journal of Numerical Methods for Heat & Fluid Flow*, Vol. 26, No. 7, 2016, pp. 2048–2065.

[29] Magrini, A., Buosi, D., and Benini, E., "Comparison of nacelle models for the evaluation of an ultra-high bypass engine aerodynamics," *AIAA SCITECH 2022 Forum*, AIAA, Reston, VA, 2022. https://doi.org/10.2514/6.2022-0205, URL https://arc.aiaa.org/doi/abs/10.2514/6.2022-0205.

[30] Magrini, A., and Benini, E., "Study of geometric parameters for the design of short intakes with fan modelling," *Chinese Journal of Aeronautics*, Vol. 35, No. 11, 2022, pp. 18–32. https://doi.org/https://doi.org/10.1016/j.cja.2022.01.018.

[31] Magrini, A., "Body Force Model Implementation of Transonic Rotor for Fan/Airframe Simulations," *Aerospace*, Vol. 9, No. 11, 2022. https://doi.org/10.3390/aerospace9110725, URL https://www.mdpi.com/2226-4310/9/11/725.